*Limnol. Oceanogr.*, 56(3), 2011, 1130–1140

doi:10.4319/lo.2011.56.3.1130

# Optical imaging of mesopelagic particles indicates deep carbon flux beneath a natural iron-fertilized bloom in the Southern Ocean

Marie-Paule Jouandet,[a,*] Thomas W. Trull,[a,b] Lionel Guidi,[c] Marc Picheral,[d] Friederike Ebersbach,[e] Lars Stemmann,[d] and Stéphane Blain[f,g]

[a] Antarctic Climate and Ecosystems Cooperative Research Center, Institute for Marine and Antarctic Studies, University of Tasmania, Hobart, Australia
[b] Commonwealth Scientific and Industrial Research Organisation Marine and Atmospheric Research, Hobart, Australia
[c] Department of Oceanography, University of Hawaii, Honolulu, Hawaii
[d] Laboratoire d'Océanographie de Villefranche, University of Pierre and Marie Curie-Paris 6, Villefranche-sur-Mer, France
[e] International Graduate School for Marine Science (GLOMAR), University of Bremen, and Alfred Wegener Institute for Polar and Marine Research, Bremerhaven, Germany
[f] University of Pierre and Marie Curie, Unit Mixed of Research (UMR) 7621, Laboratoire d'Océanographie Microbienne (LOMIC), Observatoire Océanologique de Banyuls sur Mer, France
[g] Scientific national research center, UMR 7621, LOMIC, Observatoire Océanologique, Banyuls sur Mer, France

*Abstract*

We recorded vertical profiles of size distributions of particles (ranging from 0.052 to several mm in equivalent spherical diameter) in the natural iron-fertilized bloom southeast of Kerguelen Island (Southern Ocean) and in surrounding high-nutrient, low-chlorophyll (HNLC) waters with an Under Water Video Profiler during the Kerguelen Ocean and Plateau Compared Study cruise (Jan–Feb 2005). Total particle numerical abundance and total particle volume (TPV) in the 0–200-m layer were respectively 3-fold and 20-fold higher in the bloom, and integrated TPV was correlated to integrated chlorophyll concentration. The difference persisted well into the ocean interior with a 10-fold higher TPV at 400-m depth beneath the natural iron-fertilized bloom. Below 400 m, increases in TPV values at the bloom stations reflect the suspension of bottom sediments. Bloom waters had a greater proportion of large particles from the surface to 400 m and also exhibited an increase of this proportion with depth compared to HNLC waters. Multiple visits to the bloom reference Sta. A3, suggest preferential removal of large particles as the bloom declined. Comparing our particle abundance size spectra with those observed previously in polyacrylamide gel-filled sediment traps allows us to estimate mesopelagic particle sinking rates. These results suggest that particles sink faster in the HNLC waters than beneath the bloom. The fact that sinking speeds were not a simple monotonic function of particle size and varied spatially highlights the need to go beyond parameterizations of sinking rate as a function of size alone.

The biological carbon pump is a key process influencing the atmospheric carbon dioxide ($CO_2$) concentration (Volk and Hoffert 1985), and depends on both the magnitude of primary production (PP) in the surface mixed layer and the fraction of this organic matter that is exported to depth. Artificial iron fertilization experiments have demonstrated an enhancement of PP associated with a shift in the structure of the phytoplankton community toward larger diatoms (de Baar et al. 2005), but the extent of carbon export to the ocean interior remains difficult to quantify (Boyd et al. 2007). The issue of carbon export has also been addressed in natural iron fertilization studies, which have observed an increase in shallow export compared to high-nutrient, low-chlorophyll (HNLC) surrounding waters (Blain et al. 2007; Pollard et al. 2007).

The amount of particulate organic carbon (POC) produced in the euphotic zone that is transferred through the mesopelagic zone by sinking particles depends on their sinking velocities and the rate at which they decompose or are consumed. The specific shape of the resultant POC flux profile is usually described as an empirical function of shallow export (Martin et al. 1987), but has been shown to vary from place to place (Berelson 2002; Buesseler et al. 2007*b*; Guidi et al. 2009). Flux attenuation has mainly been investigated using sediment traps, although this approach can only provide sparse observations, and may be biased by swimmer contamination, sample degradation, and hydrodynamic effects (Buesseler et al. 2007*a*). These limitations underscore the utility of indirect methods to obtain estimates of flux, such as optical observations of in situ particle concentrations (Gorsky et al. 2000) associated to the use of empirical relationship, and this is the primary approach applied in this study.

The Kerguelen Ocean and Plateau Compared Study (KEOPS) investigated a naturally iron-fertilized portion of the Southern Ocean, which is the largest HNLC region in the global ocean. The study area was located to the southeast of the Kerguelen Islands in the Indian sector of the Southern Ocean where a well-developed bloom is observed every summer in satellite chlorophyll images (Blain et al. 2007; Mongin et al. 2008). The bloom was found to be sustained by the supply of iron and major nutrients to surface waters from iron-rich deep water by vertical winter and diapycnal mixing (Blain et al. 2007). Export estimated from the seasonal surface mixed-layer carbon budget and from the $^{234}Th$ deficit method at 100 m

* Corresponding author: MariePaule.Jouandet@utas.edu.au

suggested that the carbon export was more than two-fold higher over the plateau than in adjacent HNLC waters (Jouandet et al. 2008; Savoye et al. 2008) but that the efficiency, defined as the $^{234}$Th-based export production to primary production ratio, was higher in the HNLC waters (Savoye et al. 2008). The difference appeared to be due to a higher bacterial activity in the iron-fertilized waters (Obernosterer et al. 2008). The effect of iron on the biological carbon pump in the mesopelagic zone was inferred from the distribution of excess, nonlithogenic particulate barium, which indicated lower remineralization between 125 m and 400 m beneath the bloom than in the HNLC waters (Jacquet et al. 2008). Deployment of surface-tethered free-drifting sediment traps indicated higher export from the center of the bloom than in surrounding HNLC waters, at 200-m depth (Trull et al. 2008), and optical examination of particles trapped in polyacrylamide gels suggested export was dominated by fecal pellets and fecal aggregates within the bloom (Ebersbach and Trull 2008).

These previous studies at the KEOPS site only examined export in the upper ~ 200 m. Only three free-drifting trap deployments were successful and one of these experienced technical problems (Ebersbach and Trull 2008) and, thus, could not fully assess carbon export to the ocean interior. In this paper we examine in situ particle concentrations and size spectra obtained from 25 vertical profiles using an underwater video profiler (UVP) to assess the effect of iron on the intensity of the biological carbon pump. The objectives of the present study are three-fold: (1) to estimate to what extent the Kerguelen natural iron fertilization increases the abundance of particles in the water column, in and below the surface mixed layer; (2) to see if particle size spectra evolve with depth in the bloom and in the surrounding HNLC waters in order to estimate the processes controlling the export; and (3) to investigate the response of particle sinking speeds to iron inputs, by comparison of the UVP particle abundances to those obtained from polyacrylamide gel-filled sediment traps (Ebersbach and Trull 2008).

## Methods

*Site description*—The KEOPS project has been summarized in an overview article and detailed in a special volume (Blain et al. 2007, 2008). In brief, the KEOPS cruise took place from 19 January to 13 February 2005. Satellite images (composite of moderate resolution imaging spectroradiometer [MODIS] and medium-resolution imaging-spectrometer images) were used to determine the position of the stations and indicated that the phytoplankton bloom started in November, peaked in late December, and was in decline by the time of the voyage, reaching background levels by the end of February (Blain et al. 2007; Mongin et al. 2008). Three transects (A, B, C) of 11 stations each were carried out crossing the Kerguelen Plateau and extending into the off-shelf deep waters (deep being defined as water > 1000 m; Fig. 1). These transects crossed distinct biogeochemical provinces with Sta. A1–A5 and B1–B5 in the heart of the natural iron-fertilized bloom (Fig. 1),

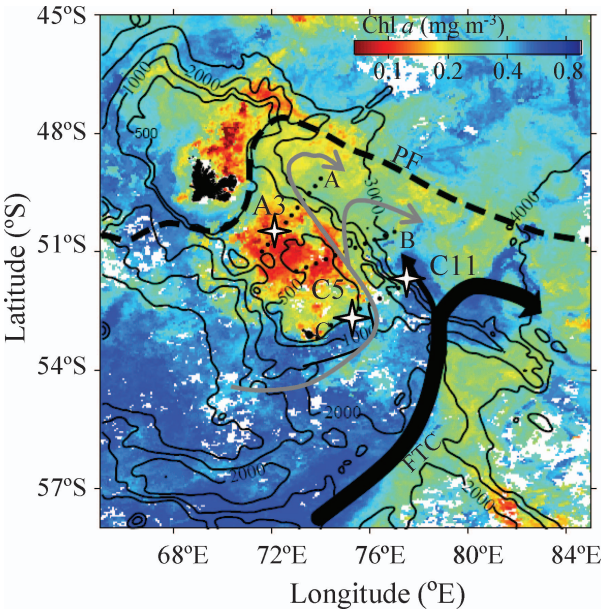


Fig. 1. Monthly mean chlorophyll concentration for January 2005 from MODIS data (adapted from Park et al. 2008*a*). The currents and fronts are from Park et al. (2008*b*). Plateau bathymetry is shown by black contours (at 500 m, 1000 m, 2000 m). The three transects (A, B, and C, each with 11 stations), are shown in black. A3 was designated as the bloom reference station and C11 as the HNLC references station (Blain et al. 2007). C5 also exhibited HNLC characteristics, and was the site of the HNLC sediment-trap deployment (Ebersbach and Trull 2008). PF: Polar Front; FTC: Fawn Trough Current.

characterized by high chlorophyll *a* (Chl *a*) and low nutrient concentrations (Blain et al. 2007; Mosseri et al. 2008) and the off shore stations (A9–A11, B9–B11, C9–C11) characterized by HNLC conditions. A3 and C11 were considered to be reference stations for the bloom and HNLC conditions, respectively (Blain et al. 2007), and were visited multiple times to examine temporal changes. Sta. A3 (50°38′S, 72°05′E) was sampled twice early in the voyage (A3–1: 22 Jan 2005, A3–2: 23 Jan 2005) and again near the end (A3–3: 12 Feb 2005), and Sta. C11 (51°39′S, 78°00′E) was visited twice (C11–1: 26 Jan 2005 and C11–2: 05 Feb 2005).

As indicated in Fig. 1, the eastward-flowing Antarctic Circumpolar Current is divided by the Kerguelen Plateau, with some flow transiting the plateau in association with the Polar Front just south of the Kerguelen Islands, and the majority flowing around the southern edge of the plateau in the Fawn Trough (Park et al. 2008*b*). This southern branch turns northward along the eastern edge of the plateau before continuing on its circumpolar path. These flows influence the intensity of the phytoplankton bloom. Sta. A1–A5 and B1–B5 on the central plateau were characterized by weak geostrophic currents (3–5 cm s$^{-1}$) and an anticyclonic flow and exhibited the highest biomass. Sta. C1, C3, and C5 were influenced by the relatively strong (up to 18 cm s$^{-1}$) northerly flow bringing HNLC waters onto this southern border of the plateau, and exhibited relatively low chlorophyll. The stations to the east of the plateau (A9–11, B9–11, C9–11) were generally in HNLC condi-

Table 1. Particle size bins used in the analysis of the UVP and gel trap images. 18 bins were used for the UVP and 9 for the gels. The values are the ESD minima for each bin, and the maximum for the largest bin. In the discussion of the UVP results, small particles refers to bins 1–10, and large particles to bins 11–18.

| Bin limits | ESD (mm) (UVP) | ESD (mm) (gel trap) |
|---|---|---|
| 1 | 0.052 | — |
| 2 | 0.066 | — |
| 3 | 0.083 | — |
| 4 | 0.105 | — |
| 5 | 0.132 | 0.155 |
| 6 | 0.166 | 0.178 |
| 7 | 0.209 | — |
| 8 | 0.264 | 0.252 |
| 9 | 0.332 | 0.357 |
| 10 | 0.419 | — |
| 11 | 0.527 | 0.505 |
| 12 | 0.665 | 0.714 |
| 13 | 0.837 | — |
| 14 | 1.055 | 1.009 |
| 15 | 1.329 | 1.427 |
| 16 | 1.674 | — |
| 17 | 2.110 | 2.019 |
| 18 | 2.66 | 2.855 |
| max. | 3.34 | — |

tions, but with somewhat higher biomass downstream of the plateau along the A and B transects than on the C transect.

All the bloom stations were dominated by the microphytoplankton size class, primarily composed of diatoms. The HNLC stations exhibited similar community structure, but with a greater contribution from the nano-phytoplankton size class (Uitz et al. 2009). The decline of the bloom during the study period was associated with a change in diatom community structure shifting from an initial bloom of *Chaetoceros hyalochaete* species to a quite monospecific bloom of *Eucampia antarctica* (Armand et al. 2008). In contrast, only small changes were observed between the two visits to the HNLC station, where *Fragilariopsis pseudonana* was the most abundant diatom and the larger open-ocean species *F. kerguelensis* dominated the diatom carbon biomass. Zooplankton communities were dominated by copepods, particularly by large- and medium-size calanoid species, at all stations but with a four-fold higher depth-integrated (0–200 m) biomass in the bloom compared to outside (Carlotti et al. 2008).

*Underwater video profiler deployments*—During the KEOPS A, B, and C transects, 25 vertical profiles, from the surface to 500 m for the plateau stations and to 1000 m for the off-shelf stations, were carried out with the Underwater Video Profiler (UVP) constructed in the Laboratoire d'Océanographie of Villefranche sur Mer. The UVP measured objects illuminated in a slab of water of known volume of 10.53 liters. The number of pixels was converted to surface areas, using the results of size and volume calibrations conducted in a seawater tank using natural particles of different types to determine the conversion between pixels to metric units (M. Picheral unpubl.). The equivalent spherical diameter (ESD) of particles larger than 0.052 mm was calculated from the particle's projected area in the image, assuming spherical shape. Images were recorded digitally by two cameras (the second camera with a higher magnification observes a portion of the illuminated volume) at a rate of 12 images $s^{-1}$ and processed with custom-made image-analysis software (Gorsky et al. 2000).

The resulting particles sizes were binned into 27 ESD intervals (from 0.052 mm to 27 mm, spaced geometrically), and concentrations were averaged over 5-m depth intervals referenced to simultaneous conductivity–temperature–depth (CTD) bio-optical data. The UVP was equipped with sensors for temperature, salinity, fluorescence, and turbidity (backscattered red light). We examined size spectra showing a minimum of 5 particles per bin and depth interval (this criterion eliminated bins $>$ 3.34 mm; Table 1) and divided each spectrum into small particles (0.052 mm $<$ ESD $\leq$ 0.527 mm) and large particles (0.527 mm $<$ ESD $<$ 3.34 mm). The particle results are presented in terms of their number and volume concentration within each size, N (No. $L^{-1}$) and V ($mm^3$ $L^{-1}$), respectively. The CTD profiles and sensor data allow the particle image statistics to be compared to physical water-column structure. We estimated surface mixed-layer depth defined as the depth where the potential density differs by 2% from the surface value (Price et al. 1978). These ranged from $\sim$ 50-m to $\sim$ 110-m depth, and are shown in Fig. 2.

## Results

*Total particle concentration and volume distributions along the A, B, and C transects*—The individual profiles of total particle number (TPN), total particle volume (TPV), and fluorescence are shown in Fig. 2, arranged according to their longitudes along the A, B, and C transects to provide a picture of the overall spatial distribution. Several broad characteristics emerge from this picture: (1) surface waters have the highest values of TPN and TPV, and these are higher over the plateau than outside; (2) TPN and TPV values decrease rapidly beneath the mixed layer; (3) values at mid-depths (200–400 m) are very low at all the stations (with the exception of C3); and (4) many stations over the plateau show near-bottom TPN enrichments (below 400 m). In the following paragraphs we examine these characteristics in more detail.

In the surface mixed layer, the maximum TPN and TPV at the bloom stations (A1, A3, A5, B1, B3, B5) averaged $1.4 \times 10^3 \pm 0.2 \times 10^3$ No. $L^{-1}$ and $183 \pm 34$ $mm^3$ $L^{-1}$, respectively. In contrast, the HNLC stations were characterized by at least three-fold lower values with TPN $<$ 500 No. $L^{-1}$ and TPV under 50 $mm^3$ $L^{-1}$. The smallest TPN ($73 \pm 15$ No. $L^{-1}$) and TPV ($1.8 \pm 0.5$ $mm^3$ $L^{-1}$) occurred at HNLC Sta. C5 and C11. The overall spatial distribution of the surface mixed-layer TPN and TPV values is similar to that for phytoplankton fluorescence (Fig. 2), and this leads to a correlation of TPV and Chl *a* when integrated over the top 200 m (Fig. 3). The correlation is largely

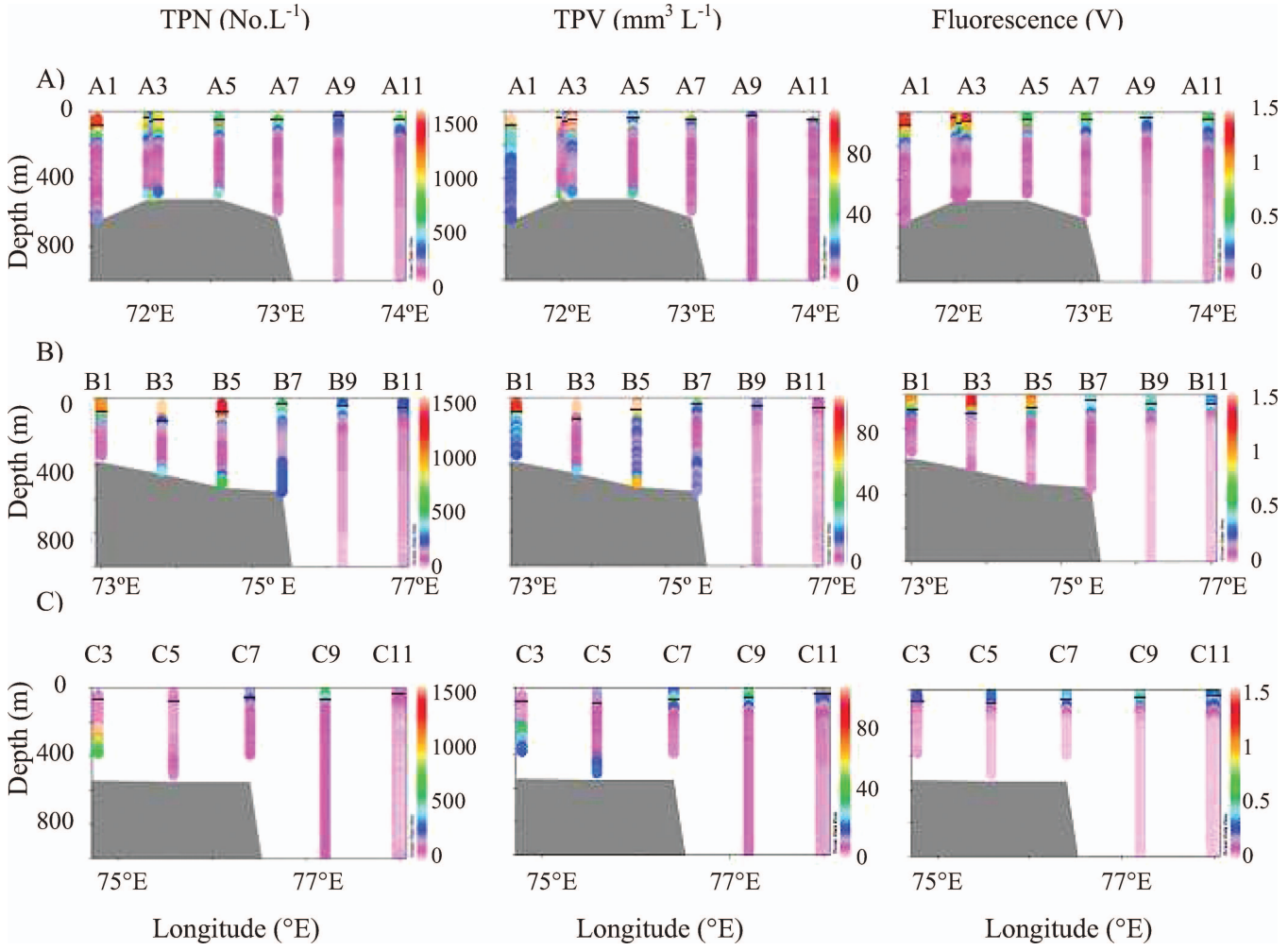


Fig. 2. Near-surface vertical distribution of the total particle number (TPN), volume (TPV), and fluorescence for transects (A) A, (B) B, and (C) C in the water column. The black lines show the mixed-layer depth.

defined by two end-members—the highest values in the bloom over the plateau including the first two visits to the A3 bloom reference station, and the lowest values at the off-plateau stations including the C11 HNLC reference station (Fig. 3). Within the subset of the bloom stations, there is less correlation, with varying Chl *a* levels accompanied by relatively constant TPV values. One possible explanation is an increase in Chl *a* levels per cell in response to self-shading in the bloom, but data to test this are not available.

Below the mixed layer, TPN and TPV both decreased very rapidly from the surface values, by a factor of 10 (TPN = 128 ± 33 No. $L^{-1}$ and TPV = 17 ± 10 $mm^3$ $L^{-1}$ at 200-m depth) at the bloom stations. Broadly similar vertical profiles occurred at the HNLC stations (Fig. 2). These strong decreases with depth also occurred in phytoplankton fluorescence (Fig. 2), suggesting that the profiles below the mixed layer (down to 200 m) are controlled by active exchange of surface and subsurface waters (as mediated by energetic internal waves and reflected in high estimates for the vertical eddy diffusivity; Park et al. 2008*a*).

Below 200 m depth, phytoplankton fluorescence is minimal, and the TPN and TPV values decrease relatively slowly, only a factor of 1.7 from 200 m to 400 m in contrast to the 10-fold decrease from surface maxima to 200-m depth. Vertical mixing is much less active at these depths, which are below the remnant temperature minimum layer at ~ 200-m depth that reflects the maximum depth of winter mixing (Blain et al. 2007). In this layer, particle populations may be controlled primarily by biological processes.

Within about 100 m from the bottom, many on-plateau stations exhibit sharp increases in TPN values, and less strongly in TPV values (Fig. 2). This presumably represents resuspension of bottom sediments, as has also been suggested based on particulate iron measurements (Chever et al. 2010). This explanation may also apply to the somewhat elevated TPN and TPV between 200 m and 400 m that was observed only at Sta. C3 (TPN ranging between 220 No. $L^{-1}$ and 502 No. $L^{-1}$, and TPV between 23 $mm^3$ $L^{-1}$ and 125 $mm^3$ $L^{-1}$), with the particles possibly derived from the shelf near Heard Island. There is no evidence of TPN or TPV increases at similar depths in any of the off-plateau stations, including Sta. A9 and B9, which are directly downstream from the plateau, suggesting that the resuspended particles are not transported far laterally.

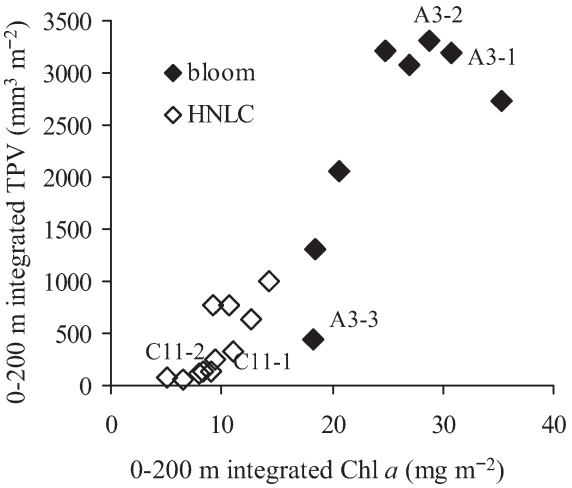


Fig. 3. Comparison of the total particle volume (TPV), to phytoplankton fluorescence integrated on the 0–200-m surface layer for all KEOPS stations.

In the sections that follow we discuss the 0–200-m and 200–400-m depth bands separately. Phytoplankton dominates TPN in the first band, and these waters exhibit strong decreases in particle number and volume with depth. Extant phytoplankton is essentially absent in the second band, and changes in particle numbers with depth are smaller and steadier. We refer to these two bands as the surface and mesopelagic layers.

For the surface layer, we focus on temporal changes related to bloom and particle formation dynamics, and for the mesopelagic layer we emphasize the estimation of the changes in particle abundances and sizes with depth to demonstrate biological or physical controls on material transfer to the ocean interior. We focus on Sta. A3 and C11, which are, respectively, reference stations for the bloom and the HNLC area (Blain et al. 2007) and also examine HNLC Sta. C5 where particle-size distributions were also determined from polyacrylamide-gel–filled sediment traps (Ebersbach and Trull 2008).

*Vertical distributions of small and large particles in the 0–200-m surface layer at the bloom and HNLC reference stations*—The vertical distributions of the small particle volumes (SPV; 0.052 mm $<$ ESD $\leq$ 0.527 mm) and large particle volumes (LPV; 0.527 mm $<$ ESD $<$ 3.34 mm) for the A3 bloom reference station (A3-1: 22 Jan 2005, A3-2: 23 Jan 2005, A3-3: 12 Feb 2005), and the HNLC stations C11 (C11-1: 26 Jan 2005; C11-2: 05 Feb 2005) and C5 are shown in Fig. 4A. This set of sites and profiles lets us examine differences between the bloom and HNLC waters, variations with depth, and changes with time. As noted above in discussing Fig. 2, the A3 bloom station has higher TPV than the HNLC stations. Fig. 4A shows that this higher TPV is accompanied by a greater proportion of large particles, throughout the water column.

Vertical distributions of SPV and LPV differed between the bloom and HNLC sites. At the A3 bloom station, LPV showed high values from the surface to $\sim$ 150-m depth before decreasing strongly. At the HNLC sites the near-surface particle abundances did not extend as deeply, dropping to low values at $\sim$ 120 m. This difference does not appear to be driven by the differences in the depth of the mixed layers, because mixed-layer depths were similar or slightly deeper at the HNLC sites (Figs. 4, 5), and generally shallower than the depths at which particle volumes decreased strongly (Fig. 4). The bloom sites exhibited double maxima in LPV values, the first one around 50 m and the second one between 100 m and 140 m, but no structure in SPV profiles. In contrast, the HNLC sites exhibited profiles with single maxima in LPV, which were echoed by SPV values, at much shallower depth (60–70 m). LPV and SPV values in these maxima were more than six-fold lower than at the bloom station.

These interesting features in the LPV and SPV distributions were correlated to the profiles of phytoplankton fluorescence and turbidity (Fig. 5). In the bloom, fluorescence profiles were also characterized by first maxima around 50 m and second maxima at 120 m although these features were not as strong as in the LPV profiles (Fig. 4). Weak maxima in fluorescence corresponding to the SPV–LPV maxima were also present for the HNLC stations. Turbidity exhibits a maximum only at the depth of the deeper LPV feature at A3. Taken together, these observations suggest that the LPV, and to a lesser degree the SPV, distributions correspond with those of phytoplankton for both the bloom and HNLC environments in surface waters.

Changes over time were minimal at the C11 HNLC reference site, but dramatic at the A3 bloom reference site between the first two visits (A3-1 and A3-2 just 1 d apart) and the last visit 20 d later (A3-3). By the time of the last A3-3 visit the LPV values had decreased more than five-fold in comparison to the A3-1 and A3-2 visits, yet the double maxima persisted. This makes it clear that the lower values were not the result of HNLC waters arriving at the bloom site, but of temporal evolution of the bloom, a perspective consistent with the slow circulation in this region (as detailed in the Methods section). The intensity of the shallow subsurface maximum at 50 m decreased with time from 160 mm$^3$ L$^{-1}$ (A3-1) to 27 mm$^3$ L$^{-1}$(A3-3) and the deeper maximum at 100–140 m from 108 mm$^3$ L$^{-1}$ (A3-1) to 20 mm$^3$ L$^{-1}$ (A3-3). The volume of small particles also decreased three-fold from 7.4 $\pm$ 0.7 mm$^3$ L$^{-1}$ to 2.2 $\pm$ 0.3 mm$^3$ L$^{-1}$.

*Vertical distributions of the large and small particle volumes in the mesopelagic layer (depth $>$ 200 m) at the bloom and HNLC reference stations*—Fig. 4B focuses on the profiles between 200-m and 400-m depth. As noted for surface waters in the previous section, large particles dominated at all sites, and contributed more strongly to total particle volume TPV, the sum of SPV and LPV, at the bloom station. The first two visits to the A3 bloom site exhibited monotonic decreases in all particle volume parameters with depth, with the steepest decrease of the LPV at A3-1. Most of the difference between A3-1 and A3-2 comes from lower LPV (12 mm$^3$ L$^{-1}$) at 200 m while LPV values were similar at 400-m depth, equal to an average of 5.4 $\pm$ 0.8 mm$^3$ L$^{-1}$ ($n$ = 2). These profiles contrast with the C11 HNLC reference site, which exhibited fairly constant

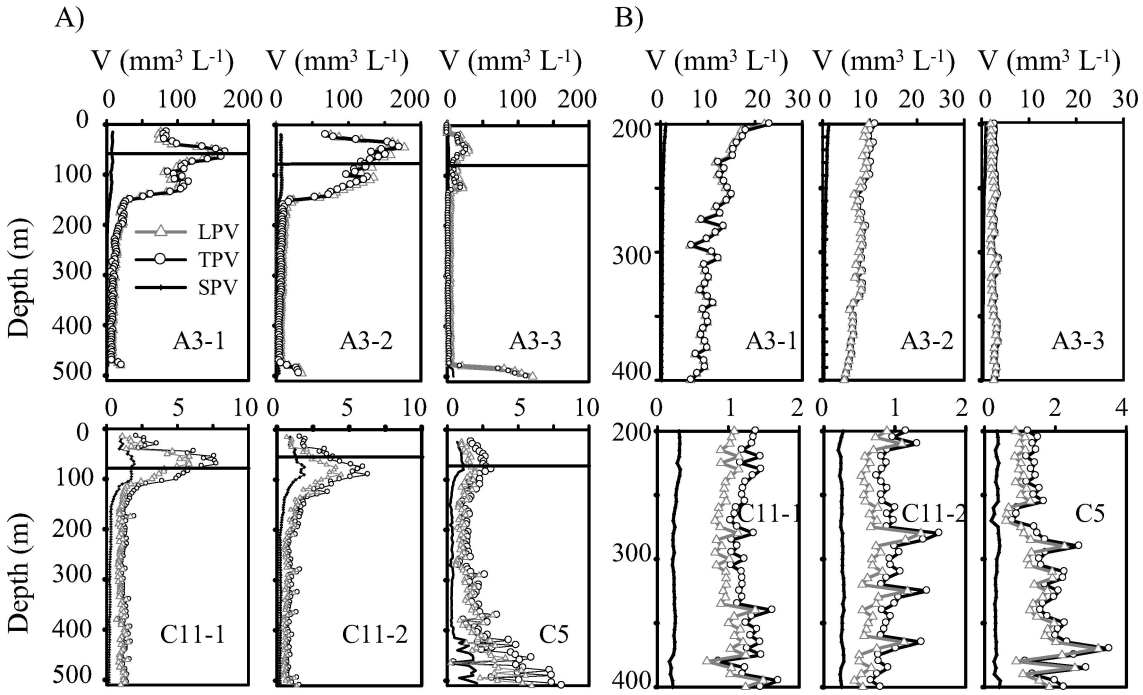


Fig. 4. (A)Vertical profiles of small (SPV), large (LPV), and total (TPV) particle volumes in the water column (0–550 m) and (B) focused in the mesopelagic layer (200–400 m) for the three visits at A3, two visits at C11, and a single visit at C5. Mixed-layer depth is indicated by a black line.

values with depth, and the C5 site at which LPV increased with depth. The last visit to A3 (A3-3), when particle concentrations were greatly diminished, showed a profile similar to the HNLC sites, with an LPV increase by 40% between 200 m and 400 m at A3-3, though still an SPV decrease with depth.

*Variations in particle size spectra*—So far we have discussed the results by binning the particle properties into two classes: small and large. In this section we discuss the continuum of particle sizes observed by the UVP, using particle size distributions. Particle number distributions ($n$) were calculated by dividing the abundance of particles ($N$) within a given bin by the width of the ESD bin, and are thus in units of No. cm$^{-4}$. The size distributions for each station are shown for three depth layers: (1) at 5-m intervals between 30 m and 70 m, where the first maximum in LPV occurs, (2) between 100 m and 140 m, where the second LPV maximum occurs, and (3) in the mesopelagic layer from 200 m to 400 m (Fig. 6). The general pattern for all stations is a decrease of abundance with increasing size (the small 'zig-zags' in the spectra are an artifact of the binning procedure, but this does not affect the total values of TPN or the slopes in the spectra). This pattern, expected from coagulation models (Jackson et al. 2005), has also been observed in previous studies (Stemmann et al. 2008).

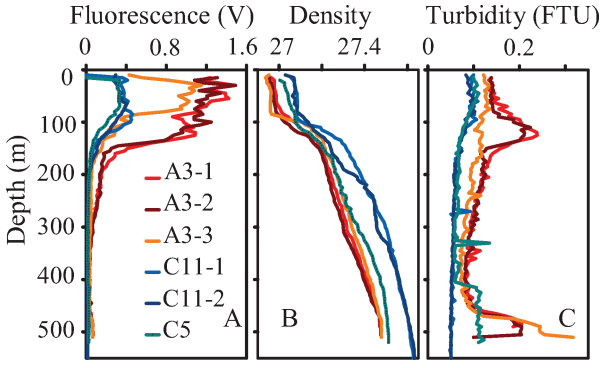


Fig. 5. (A) Density, (B) fluorescence, and (C) turbidity vertical distributions for the three visits at A3, two visits at C11, and a single visit at C5 in the water column (0–550 m).

Changes with depth in the shape of the particle number size distributions were observed for each station. To investigate these changes in detail we followed the approach of Guidi et al. (2009) and computed the slope ($m$) of the particle number size distributions according to the equation $\ln(n) = m \ln(\mathrm{ESD}) + c$. The slope $m$ is negative (because all sites have more small than large particles), and more negative values of $m$ correspond to steeper particle distributions that have a smaller proportion of large particles.

As seen on Fig. 6 (D), the particles during the two first visits of A3 were larger than in the HNLC environment and demonstrate the effect of iron on the particle size spectra. Previous study had shown an increase of size of particle in response to iron addition during the Southern Ocean Iron Release Experiment (Jackson et al. 2005). Two $m$ maxima were observed at 50 m and 120 m at A3-1 and A3-2, corresponding to an increase of the proportion of large particles. These features correspond to the LPV maxima pointed out in Fig. 4A.

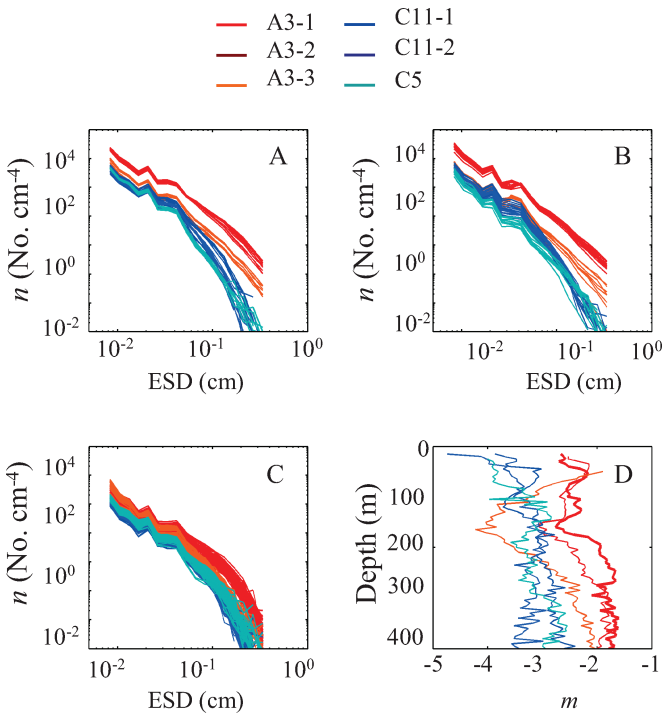


Fig. 6. Compilation of the particle size distributions for the layers (A) 30–70 m, (B) 100–140 m, and (C) 200–400 m for the three visits at A3, two visits at C11, and single visit at C5. (D) Vertical profiles of the slopes ($m$) of the particle size distributions at these sites. Grey line is the $m$ (−4) value for the global ocean from Guidi et al. (2009).

Profiles of $m$ below 200 m at A3-2, A3-3, C11-1, and C5 were characterized by a slight increase of $m$ with depth, while the $m$ profile at A3-1 was quite flat, and C11-2 was characterized by a decrease in m with depth. Similar values of $m$, and similar variations with depth, have been observed at many other sites, and those observed for the bloom station over the Kerguelen Plateau fit within the cluster-6 classification for productive waters in the classification scheme developed for a globally distributed set of observations by Guidi et al. (2009).

*Carbon export flux*—The particulate organic carbon export flux ($F_{POC}$) can be estimated from the size spectra using the empirical relationship

$$F_{POC} = Ad^b \quad (1)$$

where $A$ (12.5) and $b$ (3.81) were estimated by Guidi et al. (2008) by comparison of size spectra to deep-ocean–moored and free-floating sediment-trap POC fluxes for sites distributed around the global ocean. The value of $b$ is lower than the value of 5 that would be expected for spherical constant density particles (for which mass increases as $d^3$, and sinking speed as $d^2$), and this is consistent with increasing porosity with size for marine aggregates (Alldredge and Gotschalk 1988). We estimated fluxes in this way for the same depth and sites where free-drifting sediment traps were deployed (Ebersbach and Trull 2008; Trull et al. 2008). The resulting fluxes at 200 m, 330 m, and 400 m were highest at the first visit of A3 and decreased from 869 mg $m^{-2}$ $d^{-1}$ to 58 mg $m^{-2}$ $d^{-1}$ at 200 m, from 326 mg $m^{-2}$ $d^{-1}$ to 67 mg $m^{-2}$ $d^{-1}$ at 330 m, and from 259 mg $m^{-2}$ $d^{-1}$ to 95 mg $m^{-2}$ $d^{-1}$ at 400 m by the time of the last visit (Table 2). Considering the HNLC environment, POC fluxes were quite similar at 200 m between the different visits of C11 and C5 (32 ± 3 mg $m^{-2}$ $d^{-1}$, $n$ = 3). More variability was observed at 330 m (400 m) with values ranging from 25 mg $m^{-2}$ $d^{-1}$ (19 mg $m^{-2}$ $d^{-1}$) at C11-2 to 53 mg $m^{-2}$ $d^{-1}$ (67 mg $m^{-2}$ $d^{-1}$) at C5. These fluxes were still more than three-fold lower than fluxes in productive iron-fertilized bloom waters.

Table 2. Comparison of the POC fluxes ($F_{POC}$ in mg $m^{-2}$ $d^{-1}$) derived from particle size distributions from the UVP, particle distributions from gel-filled sediment traps (Ebersbach and Trull 2008), and direct $F_{POC}$ measurements on sediment traps (model PPS3/3, Technicap Inc., France), in the bloom and HNLC waters (Trull et al. 2008).

| | | $F_{POC}$ | | |
|---|---|---|---|---|
| Stat. | Depth | $F=Ad^b$ | Gel trap | Trap |
| A3-1 | 200 m | 869 | — | — |
| | 330 m | 326 | — | — |
| | 400 m | 259 | — | — |
| A3-2 | 200 m | 357 | — | — |
| | 330 m | 322 | — | — |
| | 400 m | 191 | — | — |
| A3-3 | 200 m | 58 | 62 | 44–48 |
| | 330 m | 67 | 8 | — |
| | 400 m | 95 | 12* | — |
| C11-1 | 200 m | 34 | — | — |
| | 330 m | 30 | — | — |
| | 400 m | 40 | — | — |
| C11-2 | 200 m | 27 | — | — |
| | 330 m | 25 | — | — |
| | 400 m | 19 | — | — |
| C5 | 200 m | 32 | 49 | 18–20 |
| | 330 m | 53 | 41 | — |
| | 400 m | 67 | 15* | — |

* flux was estimated at 430 m.

POC flux at 200 m, 330 m, and 430 m was also derived from the size of particles recorded in polyacrylamide-gel sediment traps using an empirical algorithm between the carbon content and the volume of particles (Ebersbach and Trull 2008). These values are compared to the POC flux derived from the algorithm of Guidi et al. (2008) at the last visit of A3 and C5 (Table 2). A good agreement is observed at 200 m depth for both sites, but not at deeper depths. The difference observed could result from the parameterization from Guidi et al. (2008), which assumes constant values of $A$ and $b$ for all depths.

As for the POC fluxes derived from the gel traps (Ebersbach and Trull 2008), POC fluxes derived from UVP particle sizes are higher than the POC flux measured in a drifting cylindrical sediment trap (Trull et al. 2008), suggesting that POC flux estimation from optical images tends to overestimate the flux. Nevertheless all methods show an increase of the POC flux in the bloom at 200 m in comparison to the HNLC waters. The UVP data provide new results at depth; specifically, the inferred flux is still

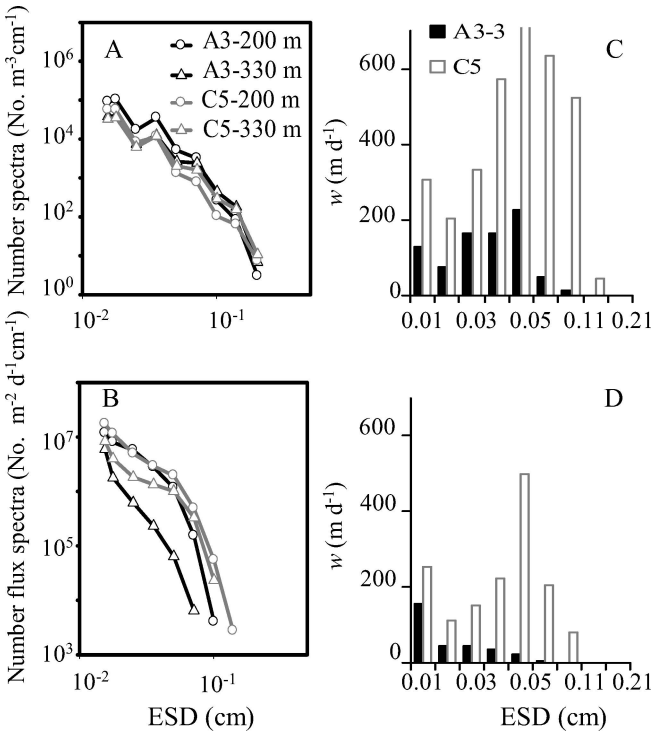


Fig. 7. (A) Number spectra for water-column particles at the trap depths from the UVP images at A3 and C5, and (B) Number flux spectra from the polyacrylamide-gel filled traps as calculated from the data of Ebersbach and Trull (2008). Settling velocities as a function of size (ESD) in the natural-iron–enriched bloom (A3) and in HNLC waters (C5) at (C) 200 m and (D) 330 m were estimated by comparing the gel-trap and UVP data.

higher at 400-m depth beneath the bloom in comparison to the surrounding HNLC waters. These results emphasize an increase of the intensity of the biological pump in a natural iron-fertilized bloom.

*Particle sinking-speed estimation*—The average particle velocity ($w_i$) for each size class, $i$, can be estimated by dividing the number flux spectra ($F_i$ in No. $m^{-2}$ $d^{-1}$ $cm^{-1}$) estimated from gel traps by simultaneous measurements of the number spectra ($n_i$ in No. $m^{-3}$ $cm^{-1}$) derived from the UVP according to

$$w_i(\mathrm{ESD}) = F_i(\mathrm{ESD}) \times [n_i(\mathrm{ESD})]^{-1} \quad (2)$$

with $i$ referring to the size class.

Simultaneous measurements of $F_i$ and $n_i$ were only realized at A3-3 and C5 at 200 m and 330 m. We didn't compute sinking speed at 430 m because particle abundance was affected by resuspension at this depth (cf Fig. 2). $F_i$ was derived from the microscopic image analyses of the gel-trap cups over the 0.155–2.855 mm particle-size interval, binning into nine size classes (Table 1; Ebersbach and Trull 2008). The 18 bins used for the number spectra determination with the UVP were combined to compare to these 9 bins (gathering bins 5–6, 6–8, 8–9, 9–11, 11–12, 12–14, 14–15, 15–17, 17–18). The resulting sinking velocities are shown in Fig. 7.

These results suggest particles sink faster in the HNLC environment compared to the bloom. This difference is driven by the higher trap-flux number spectrum at C5 compared to A3 with the greatest difference occurring at 330 m, and is, thus, subject to the possibility that it results from differences in the efficiency of particle collection by the traps at the two sites, although deployment conditions were similar (Ebersbach and Trull 2008).

The general pattern of sinking speeds as a function of size was remarkably similar for the two depths (200 m and 330 m) and two sites (A3 and C5) where direct comparison of gel-traps and UVP results was possible—a decrease of $w_i$ from the first size class to the second one followed by an increase to reach a maximum for the 0.5–0.7 mm size class, except at A3-330 m where a continuous decrease with size was observed. The fastest $w_i$ was computed at C5 with value of 1400 m $d^{-1}$, seven-fold higher than the maxima at A3. This high value results from a high number flux recorded by the gel trap while the UVP number spectrum was low. In contrast, the high values for the size class 0.5–0.7 mm at A3-200 m, C5-200 m, and C5-300 m results from a sharp decrease of $n_i$ for a similar $F_i$. The $w_i$ for particles with ESD up to 0.7 mm decrease with increasing ESD. No sinking speeds could be computed for the two largest size classes (ESD $>$ 1.4 mm) at A3-200 m and 330 m and C5-330 m because no particles this large were recorded by the gel trap. Concerning the variation of the sinking speed with depth, $w_i$ was characterized by a decrease from 200 m to 330 m with the largest decrease noticed at A3-330 m. This decrease is due to the diminution of $F_i$ (Fig. 7A).

## Discussion

*Comparison of bloom and HNLC environments*—The overall objective of this work was to assess the effect of iron on the intensity of the biological carbon pump. The UVP images clearly show that more and larger particles are present beneath the bloom than in surrounding waters, and that this extends deep into the mesopelagic ocean (to 400-m depth). Figs. 2, 3, 4A, and 5 reveal that the higher production of particles in the natural iron-fertilized bloom is linked to the stronger surface phytoplankton production. Figs. 4A, and 6 indicate that differences in particle processing also occur at mesopelagic depths. The analysis of the gel traps showed that the sinking material was dominated by fecal material at 100-m, 200-m, and 330-m depth demonstrating that the formation of large particles results mainly from grazing rather than diatom aggregation (Ebersbach and Trull 2008).

At the time of the bloom (A3-1 and A3-2) $F_{POC}$ and LPV in the mesopelagic waters were characterized by decreases with depth associated with an increase of the proportion of large particles. Several mechanisms could account for this pattern; among them, the most likely are particle alteration processes such as fragmentation and–or remineralisation and–or zooplankton grazing. No increase of small particle volume was observed in the mesopelagic layer and, thus, fragmentation seems unlikely. Microbial consumption of particles is also known to affect particle geometry and to decrease particle volume (Stemmann et al. 2004) but this

process is unlikely to promote an increase of the fraction of large particles and remineralisation rate based on excess barium concentrations was low in the mesopelagic zone (Jacquet at al. 2008). Consumption by zooplankton appears most likely to be responsible for the decrease of LPV and for the increase of the proportion of larger particles by repackaging through the excretion of larger fecal pellets. Of course, the shift toward a greater proportion of larger particles with depth could also reflect temporal change in the delivery of particles produced at the surface, with production of fewer smaller particles at the end of the bloom as seen on Fig. 6 at the last visit of A3.

The last visit at A3 was characterized by an increase of TPV with depth in the mesopelagic layer, which could reflect the decline in particle delivery from the bloom above, or temporal variability between the timing of production in surface and export at depth as previously described in Savoye at al. (2008). Another contributing explanation could come from the decrease of sinking speed with depth (shown in Fig. 7), because a slowdown in particle settling would lead to an accumulation with depth proportional to the diminution of the settling rate.

*Sinking speed*—The sinking speed computed using gel trap and UVP data was lower in the natural iron-fertilized bloom compared to the HNLC waters for the whole size spectrum. Phytoplankton community was dominated by diatoms in the bloom and in the HNLC waters but with difference in silicification degree (Mosseri et al. 2008). The stronger silicification in the HNLC waters could contribute to the high sinking speed in the HNLC waters, via an increase of ballast. Higher porosity in the bloom-derived particles, as a result of differing grazing and aggregation processes could also contribute to this result.

The fact that the sinking speed is not a simple monotonic function of particle size was a surprising result and was also observed by McDonnell and Buesseler (2010) in the Southern Ocean (West Antarctic Peninsula) using the same computational method. Nevertheless the variation of sinking speed observed in this study is different from the one reported in McDonnell and Buesseler (2010). The sinking speed was maximal for the middle size class (0.5–0.7 mm) in our study whereas they computed maximal sinking speeds for the smallest and largest size classes, dominated by diatom aggregates and krill fecal pellets, respectively. These results, in addition to comparison with sinking speeds from the literature (Fig. 8) highlight the need to go beyond parameterizations of sinking rate as a function of size alone, as derived previously from in situ studies (Alldredge and Gotschalk 1989; Syvitski et al. 1995) and models (Stokes law, Stemmann et al. 2004).

Comparison between the study of McDonnell and Buesseler (2010) and our results shows also discrepancy in the variation of sinking speed with depth. Sinking speed was characterized by an increase with depth in waters of the Antarctic Peninsula while our study demonstrated a decrease of the sinking speed with depth, by more than a factor of 2. This decrease was unexpected considering the study of Berelson (2002) that argued for increasing sinking rates with depth based on deep-ocean—moored traps. This

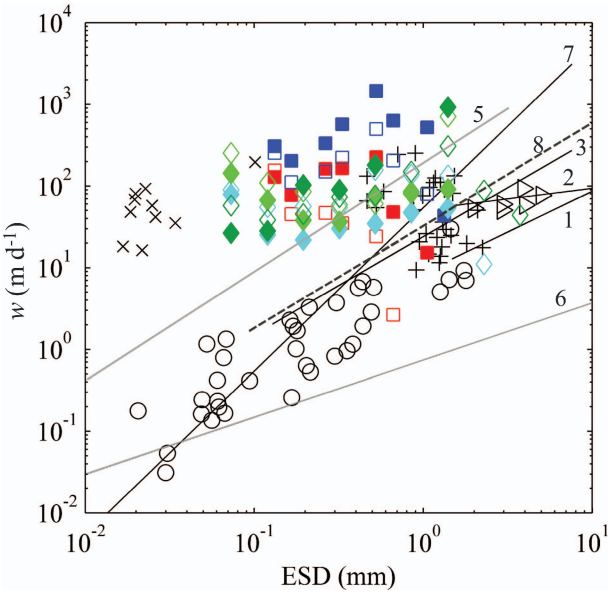


Fig. 8. Comparison of particle sinking velocities estimated here (filled red square: A3 200 m, open red square: A3 330 m; filled blue square: C5 200 m; open blue square: C5 330 m) with previous results using the same approach from McDonnell and Buesseler (2010; PS1 150 m: filled turquoise diamond; PS1 250 m: open turquoise diamond; PS2 200 m: filled green diamond; PS2 300 m: open green diamond, PS3 150 m: filled dark green diamond; PS3 250 m: open dark green diamond) and other approaches (from Guidi et al. [2008]; circle: Smayda [1970]; triangle: Shanks and Trent [1980]; cross: Carder et al. [1982]; plus sign: Azetsu-Scott and Johnson [1992]; empirical relationships: 1—Alldredge and Gotschalk [1988]; 2—Alldredge and Gotschalk [1989]; 3—Syvitski et al. [1995]). Settling velocities calculated using the coagulation model (Stemmann et al. 2004) with different parameter values (5—particle excess density ($\Delta\rho$ = 0.08, fractal dimension (D) = 2.33; 6—$\Delta\rho$ = 0.01, D = 1.79) are also reported. The regression line 7 is the settling speed predicted by Stokes Law. The dashed line 8 is the settling speed calculated in Guidi et al. (2008).

finding is of crucial importance, because parameterizations consistent with increasing sinking speed (Kriest and Oschlies 2008) or constant sinking speed (Gregg et al. 2003) for flux attenuation have been used in large-scale biogeochemical models to explain regional variations in the biological pump. The decrease of the sinking speed in the present study is associated to an increase of the proportion of larger particles (cf Fig. 6), which would be consistent with a decrease of porosity in large particles (Ploug et al. 2008). Overall, the observed sinking-speed variability with environment and depth indicates that global relationships between particle concentrations and flux are oversimplifications for the estimation of POC flux.

Our sinking-speed estimation approach is admittedly indirect, and it is perhaps possible that the complex relationships between the size of the particles and their sinking speed results from low efficiency of the gel trap to collect large particles or–and the fact that some unknown fraction of the larger particles seen by the UVP is not sinking (e.g., zooplankton). These estimations of sinking rate also assume that no sorting or particle size conversions occur

during trapping, which is debateable (Buesseler et al. 2007*a*), although the fine and complex structures observed in the gel traps favor relatively undisturbed collection. Focusing only on the small size classes (ESD $< 0.5$ mm), where UVP and gel trap are most likely to sample the same material, also shows no correlation between sinking speed and size.

*Acknowledgments*

Thanks to the Kerguelen Ocean and Plateau Compared Study (KEOPS) shipboard science team and the officers and crew of R/V *Marion Dufresne* for their efforts. Australian involvement in KEOPS and this postvoyage project received support from the Australian Commonwealth Cooperative Research Center Program and Australian Antarctic Sciences Award 1156. L. G. contribution was partly supported by the Center for Microbial Oceanography, Research and Education (National Science Foundation grant EF-0424599) and the Gordon and Betty Moore foundation. We also thank two anonymous referees for their valuable comments.

## *References*

Alldredge, A. L., and C. Gotschalk. 1988. In situ settling behavior of marine snow. Limnol. Oceanogr. **33:** 339–351, doi:10.4319/lo.1988.33.3.0339

———, and ———. 1989. Direct observations of the mass flocculation of diatom blooms: Characteristics, settling velocities and formation of diatom aggregates. Deep-Sea Res. **36:** 159–171.

Armand, L. K., V. Cornet-Barthaux, J. Mosseri, and B. Quéguiner. 2008. Late summer diatom biomass and community structure on and around the naturally iron-fertilized Kerguelen Plateau in the Southern Ocean. Deep-Sea Res. II **55:** 653–676, doi:10.1016/j.dsr2.2007.12.031

Azetsu-Scott, K., and B. D. Johnson. 1992. Measuring physical characteristics of particles: A new method of simultaneous measurement for size, settling velocity and density of constituent matter. Deep-Sea Res. I **39:** 1057–1066, doi:10.1016/0198-0149(92)90039-V

Berelson, W. M. 2002. Particle settling rates increase with depth in the ocean. Deep-Sea Res. II **49:** 237–251, doi:10.1016/S0967-0645(01)00102-3

Blain, S., and others. 2007. Effect of natural iron fertilization on carbon sequestration in the Southern Ocean. Nature **446:** 1070–1074, doi:10.1038/nature05700

———, and T. W. Trull. 2008. The natural iron fertilization experiment KEOPS (Kerguelen Ocean and Plateau Compared Study): An overview. Deep-Sea Res. II **55:** 559–565, doi:10.1016/j.dsr2.2008.01.002

Boyd, P. W., and others. 2007. Mesoscale iron enrichment experiments 1993–2005: Synthesis and future directions. Science **315:** 612–617, doi:10.1126/science.1131669

Buesseler, K. O., and others. 2007*a*. An assessment of the use of sediment traps for estimating upper ocean particle fluxes. J. Mar. Res. **65:** 345–416.

———, and ———. 2007*b*. Revisiting carbon flux through the ocean's twilight zone. Sciences **316:** 567–570, doi:10.1126/science.1137959

Carder, K. L., R. G. Steward, and P. R. Betzer. 1982. In situ holographic measurements of the sizes and settling rates of oceanic particulates. J. Geophys. Res. **87:** 5681–5685, doi:10.1029/JC087iC08p05681

Carlotti, F., D. Thibault-Botha, A. Nowaczyk, and D. Lefèvre. 2008. Zooplankton community structure, biomass and role in carbon fluxes during the second half of a phytoplankton bloom in the Eastern sector of the Kerguelen shelf (January–February 2005). Deep-Sea Res. II **55:** 720–733, doi:10.1016/j.dsr2.2007.12.010

Chever, F., G. Sarthou, E. Bucciarelli, S. Blain, and A. R. Bowie. 2010. An iron budget during the natural iron fertilization experiment KEOPS (Kerguelen Islands, Southern Ocean). Biogeosciences **7:** 455–468, doi:10.5194/bg-7-455-2010

De Baar, H. J. W., and others. 2005. Synthesis of iron fertilization experiments. J. Geophys. Res.-Oceans **110:** C09S16, doi:10.1029/2004JC002601

Ebersbach, F., and T. W. Trull. 2008. Sinking particle properties from polyacrylamide gels during KEOPS: Controls on carbon export in an area of persistent natural iron inputs in the Southern Ocean. Limnol. Oceanogr. **53:** 212–224, doi:10.4319/lo.2008.53.1.0212

Gorsky, G., M. Picheral, and L. Stemmann. 2000. Use of the underwater video profiler for the study of aggregate dynamics in the North Mediterranean. Estuar. Coast. Shelf Sci. **50:** 121–128, doi:10.1006/ecss.1999.0539

Gregg, W., P. Ginoux, P. Schopf, and N. Casey. 2003. Phytoplankton and iron: Validation of a global three-dimensional ocean biogeochemical model. Deep-Sea Res. II **50:** 3143–3169, doi:10.1016/j.dsr2.2003.07.013

Guidi, L., G. A. Jackson, L. Stemmann, J. C. Miquel, M. Picheral, and G. Gorsky. 2008. Relationship between particle size distribution and flux in the mesopelagic zone. Deep-Sea Res. I **55:** 1364–1374, doi:10.1016/j.dsr.2008.05.014

———, and others. 2009. Effects of phytoplankton community on production, size and export of large aggregates: A world-ocean analysis. Limnol. Oceanogr. **54:** 1951–1963, doi:10.4319/lo.2009.54.6.1951

Jackson, G. A., A. M. Waite, and P. W. Boyd. 2005. Role of algal aggregation in vertical carbon export during SOIREE and in other low biomass environments. Geophys. Res. Lett **32:** L13607, doi:10.1029/2005GL023180

Jacquet, S. H. M., F. Dehairs, N. Savoye, I. Obernosterer, U. Christaki, C. Monnin, and D. Cardinal. 2008. Mesopelagic organic carbon remineralization in the Kerguelen Plateau region tracked by biogenic particulate Ba. Deep-Sea Res. II **55:** 868–879, doi:10.1016/j.dsr2.2007.12.038

Jouandet, M. P., S. Blain, N. Metzl., C. Brunet, T. W. Trull, and I. Obernosterer. 2008. A seasonal carbon budget for a naturally iron-fertilized bloom over the Kerguelen Plateau in the Southern Ocean. Deep-Sea Res. II **55:** 856–867, doi:10.1016/j.dsr2.2007.12.037

Kriest, I., and A. Oschlies. 2008. On the treatment of particulate organic matter sinking in large-scale models of marine biogeochemical cycles. Biogeosciences **5:** 55–72, doi:10.5194/bg-5-55-2008

Martin, J. H., G. A. Knauer, D. M. Karl, and W. W. Broenkow. 1987. VERTEX: Carbon cycling in the northeast Pacific. Deep-Sea Res. I **43:** 267–285, doi:10.1016/0198-0149(87)90086-0

McDonnell, A. M. P., and K. O. Buesseler. 2010. Variability in the average sinking velocity of marine particles. Limnol. Oceanogr. **55:** 2085–2096, doi:10.4319/lo.2010.55.5.2085

Mongin, M., E. Molina, and T. W. Trull. 2008. Seasonality and scale of the Kerguelen Plateau phytoplankton bloom: A remote sensing and modeling analysis of the influence of natural iron fertilization in the Southern Ocean. Deep-Sea Res. II **55:** 880–892, doi:10.1016/j.dsr2.2007.12.039

Mosseri, J., B. Quéguiner, L. Armand, and V. Cornet-Barthaux. 2008. Impact of iron on silicon utilization by diatoms in the Southern Ocean: A case study of the Si/N cycle decoupling in a naturally iron-enriched area. Deep-Sea Res. II **55:** 801–819, doi:10.1016/j.dsr2.2007.12.003

Obernosterer, I., U. Christaki, D. Lefèvre, P. Catala, F. Van Wambeke, and P. Lebaron. 2008. Rapid bacterial mineralization of organic carbon produced during a phytoplankton bloom induced by natural iron fertilization in the Southern Ocean. Deep-Sea Res. II **55:** 777–789, doi:10.1016/j.dsr2.2007.12.005

Park, Y. H., J. L. Fuda, I. Durand, and A. C. Naveira Garabato. 2008*a*. Internal tides and vertical mixing over the Kerguelen Plateau. Deep-Sea Res. II **55:** 583–593.

———, F. Roquet, J. L. Fuda, and I. Durand. 2008*b*. Large scale circulation over and around the Kerguelen Plateau. Deep-Sea Res. II **55:** 566–581, doi:10.1016/j.dsr2.2007.12.030

Ploug, H., M. H. Iversen, and G. Fischer. 2008. Ballast, sinking velocity, and apparent diffusivity within marine snow and zooplankton fecal pellets: Implications for substrate turnover by attached bacteria. Limnol. Oceanogr. **53:** 1878–1886, doi:10.4319/lo.2008.53.5.1878

Pollard, R. T., H. J. Venables, J. F. Read, and J. T. Allen. 2007. Large-scale circulation around the Crozet Plateau controls an annual phytoplankton bloom in the Crozet Basin. Deep-Sea Res. II **54:** 1915–1929, doi:10.1016/j.dsr2.2007.06.012

Price, J. F., C. N. K. Mooers, and J. C. Van Leer. 1978. Observation and simulation of storm-induced mixed-layer deepening. J. Phys. Oceanogr. **8:** 582–599, doi:10.1175/1520-0485(1978)008<0582:OASOSI>2.0.CO;2

Savoye, N., T. W. Trull, S. H. M. Jacquet, J. Navez, and F. Dehairs. 2008. $^{234}$Th-based export fluxes during a natural iron fertilization experiment in the Southern Ocean (KEOPS). Deep-Sea Res. II **55:** 841–855, doi:10.1016/j.dsr2.2007.12.036

Shanks, A. L., and J. D. Trent. 1980. Marine snow-sinking rates and potential role in vertical flux. Deep-Sea Res. **27:** 137–143, doi:10.1016/0198-0149(80)90092-8

Smayda, T. J. 1970. The suspension and sinking of phytoplankton in the sea (RV). Oceanogr. Mar. Biol. **8:** 353–414.

Stemmann, L., D. Eloire, A. Sciandra, G. A. Jackson, L. Guidi, M. Picheral, and G. Gorsky. 2008. Volume distribution for particles between 3.5 to 2000 $\mu$m in the upper 200 m region of the South Pacific Gyre. Biogeosciences **5:** 299–310, doi:10.5194/bg-5-299-2008

———, G. A. Jackson, and G. Gorsky. 2004. A vertical model of particle size distributions and fluxes in the midwater column that includes biological and physical processes—part II: Application to a three-year survey in the NW Mediterranean Sea. Deep-Sea Res. I **51:** 885–908, doi:10.1016/j.dsr.2004.03.002

Syvitski, J. P. M., K. W. Asprey, and K. W. G. Leblanc. 1995. In-situ characteristics of particles settling within a deep-water estuary. Deep-Sea Res. II **42:** 223–256, doi:10.1016/0967-0645(95)00013-G

Trull, T. W., D. Davies, and K. Casciotti. 2008. Insights into nutrient assimilation and export in naturally iron-fertilized waters of the Southern Ocean from nitrogen, carbon and oxygen isotopes. Deep-Sea Res. II **55:** 820–840, doi:10.1016/j.dsr2.2007.12.035

Uitz, J., H. Claustre, B. Griffiths, J. Ras, and V. Sandroni. 2009. A phytoplankton class-specific primary production model applied to the Kerguelen Islands region (Southern Ocean). Deep-Sea Res. I **56:** 541–560, doi:10.1016/j.dsr.2008.11.006

Volk, T., and M. I. Hoffert. 1985. Ocean carbon pumps: Analysis of relative strengths and efficiencies in ocean-driven atmospheric $CO_2$ changes, p. 99–110. *In* E. T. Sundquist and W. S. Broecker [eds.], The carbon cycle and atmospheric $CO_2$: Natural variations archean to present. American Geophysical Union.

*Associate editor: Mikhail V. Zubkov*

*Received: 19 April 2010*
*Accepted: 13 December 2010*
*Amended: 10 February 2011*